

🍷 CrimEdit: Controllable Editing for Counterfactual Object Removal, Insertion, and Movement

Boseong Jeon^{*}, Junghyuk Lee^{*}, Jimin Park, Kwanyoung Kim,
Jingi Jung, Sangwon Lee, Hyunbo Shim
Samsung Research

{bf.jeon, j114.lee, jm2010.park, k-0.kim, jingi.jung, sw96.lee, hyunbo9.shim}@samsung.com

Abstract

Recent works on object removal and insertion have enhanced their performance by handling object effects such as shadows and reflections, using diffusion models trained on counterfactual datasets. However, the performance impact of applying classifier-free guidance to handle object effects across removal and insertion tasks within a unified model remains largely unexplored. To address this gap and improve efficiency in composite editing, we propose CrimEdit, which jointly trains the task embeddings for removal and insertion within a single model and leverages them in a classifier-free guidance scheme—enhancing the removal of both objects and their effects, and enabling controllable synthesis of object effects during insertion. CrimEdit also extends these two task prompts to be applied to spatially distinct regions, enabling object movement (repositioning) within a single denoising step. By employing both guidance techniques, extensive experiments show that CrimEdit achieves superior object removal, controllable effect insertion, and efficient object movement—without requiring additional training or separate removal and insertion stages.

1. Introduction

Diffusion probabilistic models have recently emerged as a powerful class of generative models, achieving remarkable performance in high-quality image synthesis [9, 15, 21, 22, 24]. Their scalability and flexible conditioning have led to widespread adoption in computer vision and graphics. Image editing has emerged as a particularly compelling application, offering the ability to make precise, realistic, and controllable modifications to a visual content, such as inpainting [4, 13, 18, 35, 37], object composition [29, 36], relighting [12, 40], and object repositioning [19, 32].

Object insertion, removal, and repositioning are fundamental image editing tasks that require not only altering

image content in the target region, but also preserving consistency with the surrounding scene. High-quality editing in these tasks depends on three key factors: 1) addressing visual effects such as shadows, lighting, and reflections introduced by objects, 2) providing adjustable editing guided by user preferences, and 3) versatility of a model for efficient deployment to users without the need to maintain multiple task-specific models.

To enable more realistic image editing, it is crucial to account for object-induced visual effects that contribute to the overall coherence of a scene. To this end, recent works [16, 33, 34, 39] have utilized counterfactual datasets [25], which contain paired examples of original and edited images with consistent scene layout and lighting. These datasets provide explicit supervision for learning how object presence or absence affects the surrounding visual context.

Another key aspect of image editing is controllability—specifically, the ability to adjust the intensity and characteristics of visual effects through a simple tuning process. For example, it is desirable to let users control the size of the shadow cast when inserting an object under sunlight. To address controllability in diffusion-based models, PowerPoint [42] introduced a prompt-learning framework and applied classifier-free guidance (CFG) between prompts to enable more directed generation. While effective in guiding content within specified regions, this approach is limited to in-mask editing and does not account for scene-level object effects such as shadows. The controllability and the role of task-specific guidance remain underexplored in conditional models trained with supervision on counterfactual datasets.

In practical applications, such as modern smartphone photo editors with a limited memory, users expect a seamless editing experience that supports multiple operations, such as object removal and insertion, within a single interface [3, 27]. While several prior studies [34, 39] have utilized counterfactual datasets to tackle both tasks, they typically rely on separate models for each. ObjectMover [38] takes a step toward unification by training a single model

^{*}Equal contribution

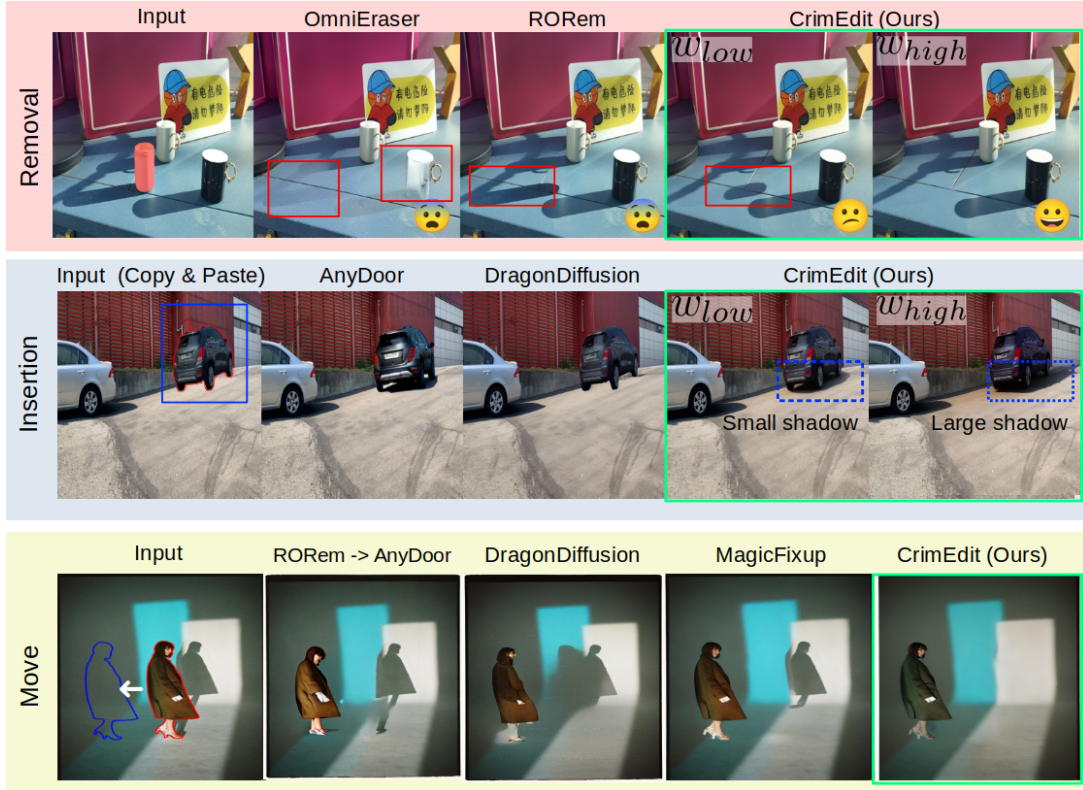


Figure 1. CrimEdit serves as a unified model to perform three tasks: object removal, insertion, and movement. By leveraging guidance between the task embeddings of removal and insertion, CrimEdit enhances removal quality and enables controllable effect generation for the insertion task. w_{low} and w_{high} denote the low and high guidance scales, respectively. For object movement, spatial guidance allows CrimEdit to perform the task in a single denoising step—without requiring separate removal and insertion phases or additional training on a movement dataset.

for both object removal and insertion, while accounting for object effects using video data. However, ObjectMover relies on additional video footage for training, which increases data collection overhead and limits scalability. It also does not fully harness the potential of multi-task conditional models, such as through CFG in the conditional embeddings for fine-grained control.

To tackle the key challenges outlined above, we propose **CrimEdit**, a unified framework for Controllable editing of counterfactual object Removal, Insertion, and Movement. Leveraging only open-sourced counterfactual image dataset [25], we first train a single diffusion model conditioned on two distinct task embeddings to perform realistic object removal and insertion within a unified architecture. We introduce a novel guidance mechanism, *Cross-Task Guidance (CTG)*, which applies classifier-free guidance between the two task embeddings. By modulating the CTG scale, our model achieves improved object removal—including associated effects such as shadows and reflections—and enables controllable synthesis of object effects during insertion. To fully exploit task condi-

tions trained within a single model, CrimEdit further proposes *Spatial CTG (S-CTG)*, which applies CTG into spatially distinct regions. This enables simultaneous object removal and insertion in a single denoising step. Without additional training for object movement, S-CTG effectively supports object repositioning while preserving realism in object-related effects. In summary, our main contributions are as follows:

- Leveraging a network trained on both complementary tasks of object removal and insertion, we propose a novel guidance technique, **CTG**, which controls the magnitude of one task by using the conditional embeddings of the other as negative guidance.
- By introducing **Spatial-CTG (S-CTG)**, which applies guidance to spatially distinct regions, we demonstrate that the model can perform object movement—or any task requiring simultaneous removal and insertion—in a single inference step, without the need for a dedicated training dataset.
- Through extensive experiments, we demonstrate that CrimEdit achieves state-of-the-art performance on object

removal, insertion, and movement tasks, outperforming baselines specifically designed for each individual task.

2. Related Works

This section reviews related works on object removal, insertion, and movement. A comparative summary is provided in Table 1.

2.0.1. Object Removal

Recent diffusion-based image inpainting models [4, 13, 18, 35] generate visually plausible content in missing or masked regions. As the naive inpainting models often produce unwanted random objects inside masks, some works have proposed removal-oriented approaches using either conditional embeddings [10, 42] or inversion-based attention reweighting [30, 37].

To enable more realistic object removal, approaches such as ObjectDrop [34], RORem [16], and OmniEraser [33] utilize counterfactual datasets [25], which contain image pairs with and without the target object. These approaches can remove not only the object itself but also its associated visual effects within the target mask region. However, guidance techniques specifically designed for counterfactual models remain underexplored. Existing methods often rely on manually crafted prompts such as 'empty' or 'background' to suppress object regeneration, but such approach tends to be ineffective in general scenarios.

2.0.2. Object Insertion

Object insertion is to place an object from a reference image into a target image, achieving color harmonization and realistic visual effects while preserving the object’s identity. Prior works [7, 8, 29, 36] extract visual features from the reference image as conditioning inputs to the diffusion model. While these methods enable object synthesis with deformations, they often struggle to preserve fine-grained identity details and frequently produce inaccurate visual effects. To improve the realism of synthesized effects, recent approaches [34, 39] leveraged counterfactual datasets and bootstrapped models originally trained for object removal. However, these methods typically train separate models for removal and insertion, limiting their efficiency for multi-purpose editing. Although OmniPaint [39] attempts to regulate effect synthesis via loss weighting during training, such control is not adjustable at inference time.

2.0.3. Object Movement

We consider the task of object movement (repositioning), where an object and its associated effects are removed from their original location and synthesized at a new location (see the last row of Figure 1). Several previous methods [31, 32] adopt a multi-stage pipeline consisting of object removal followed by harmonized insertion. This approach incurs the cumulative computational cost of both stages, as high visual

	R	I	M	Eff.	Img. Data	Task Guidance
PowerPaint	✓	✗	✗	✗	✓	✓
FunEditor	✓	✓	✓	✗	✓	✗
RORem & OmniEraser	✓	✗	✗	✓	✓	✗
ObjectDrop	✓	✓	✗	✓	✓	✗
OmniPaint	✓	✓	✗	✓	✓	✗
ObjectMover	✓	✓	✓	✓	✗	✗
CrimEdit	✓	✓	✓	✓	✓	✓

Table 1. Comparison of capabilities across methods. **R**, **I**, and **M** indicate whether removal, insertion, and movement are supported within a single denoising step. **Img. Data** indicates that the model was trained on an image dataset.

quality must be ensured independently in each phase. Drag-style editing techniques [19, 20] enable object movement in a single stage, but they require intensive computation and often suffer from background artifacts such as pixel dragging.

In contrast, FunEditor [26] adopts cross-attention (CA) masking to perform the task more efficiently, applying a removal prompt to the original region and insertion prompts to the destination. This enables object movement within a single denoising step. However, it does not address object-associated visual effects. Moreover, the CA strategy is effectively equivalent to using conditional diffusion outputs without any guidance techniques such as CFG. Other works [2, 38] leverage video footage where the target object is moved across frames to naturally capture repositioning. However, collecting such datasets is expensive and introduces challenges such as unintended background changes, shifts in camera viewpoint or lighting, and deformation particularly for non-rigid targets like humans [38].

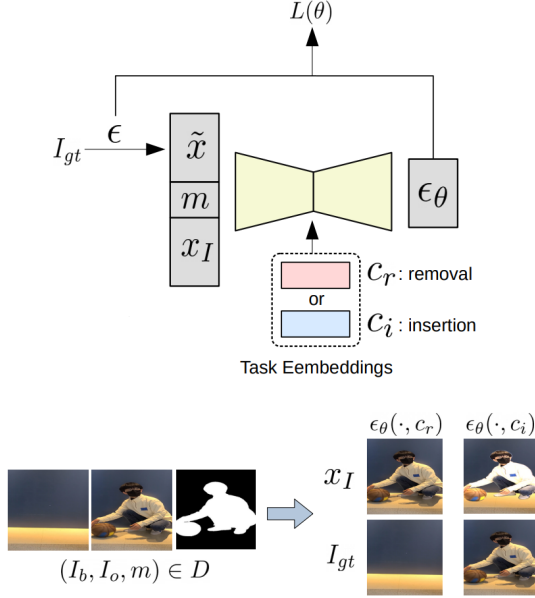
3. Method

3.1. Formulation

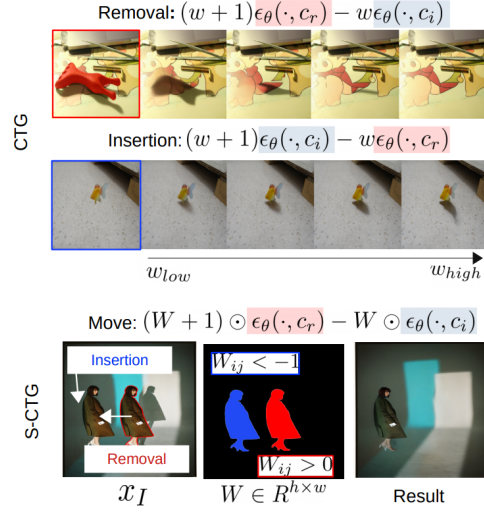
3.1.1. Task Definitions

We build CrimEdit by developing a single diffusion model ϵ_θ capable of performing the following three tasks:

- **Removal:** Given an image x_I and a object-tight mask m , ϵ_θ removes the objects within the masked region along with their visual effects, such as shadows and reflections. Additionally, it offers user-controllable options to enhance the quality of removal.
- **Insertion:** Given a copy-and-paste image x_I and a mask m indicating the pasted region, ϵ_θ harmonizes the area by adapting local lighting and synthesizing plausible visual effects. We focus on a strict identity-preserving scenario,



(a) Training on removal and insertion tasks



(b) Inference for removal, insertion, and move

Figure 2. Using counterfactual D and constant embeddings c_r and c_i , we train the diffusion network ϵ_θ on two contrasting tasks: removal and insertion. Based on $\epsilon_\theta(\cdot, c_r)$ and $\epsilon_\theta(\cdot, c_i)$, we propose cross-task guidance (CTG) which leverages classifier free guidance to better perform each task by using the other embeddings as the negative guidance. By proposing Spatial-CTG (S-CTG), we perform the two tasks in spatially different regions at a single denoising step, achieving the object movement task without additional training.

where m corresponds exactly to the pasted pixels without any deformation. Users are also provided with control over the intensity and extent of visual effects.

- **Movement:** Given an image, we assume a set of pixels \mathcal{P}_r representing the object to be moved and a set \mathcal{P}_i indicating the insertion region. Their shapes are constrained to be identical, without deformation. The input image x_I contains the object already pasted at \mathcal{P}_i , and the mask m has non-zero values only over \mathcal{P}_r and \mathcal{P}_i . The model ϵ_θ removes the object and its associated visual effects from \mathcal{P}_r , while harmonizing the pasted region and synthesizing plausible effects at \mathcal{P}_i . Notably, the model performs both removal and insertion within a single denoising step, without separate processing phases.

3.1.2. Model

In a similar manner to recent works [16, 34, 41], CrimEdit is built by fine-tuning the SDXL-inpainting model [22]. As shown in Figure 2-(a), the generator is defined as $\epsilon_\theta(x, t, x_I, m, c)$, where x is the noisy image, m is a binary mask, x_I is the conditional image, c is the prompt embedding, and t denotes the denoising step. To simplify notation, we denote identical notation for both pixel- and latent-space representations of images.

3.1.3. Dataset

For fine-tuning, CrimEdit uses only the RORD dataset [25], which provides a set of triplets $\mathcal{D} = \{(I_b, I_o, m)\}$. Here, I_b refers to an image without the target object, while I_o includes the object (see the bottom of Figure 2-(a)). Since the original mask provided by the dataset is defined by coarse polygon shapes rather than object-tight boundaries, we compute a refined mask m by extracting segmentation pixel groups contained within the polygon to ensure robust model performance.

3.2. Training CrimEdit

This section describes the training procedure for ϵ_θ on object removal and insertion tasks. To eliminate the reliance on manually crafted text prompts, ϵ_θ is trained using two fixed embeddings: c_r for removal and c_i for insertion. The model is trained to reconstruct the ground-truth image I_{gt} given a noisy input \tilde{x} and a conditional image x_I . We adopt the standard denoising diffusion loss:

$$\mathcal{L}(\theta) = E_{t \sim [0, T], \epsilon \sim \mathcal{N}(0, I)} \left[\sum \|\epsilon_\theta(\tilde{x}, t, x_I, m, c) - \epsilon\|^2 \right] \quad (1)$$

where $\tilde{x} = \alpha_t I_{gt} + \sigma_t \epsilon$.

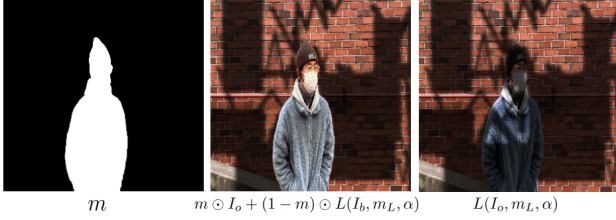


Figure 3. Shadow augmentation for enhanced local light consistency of insertion task in Equation (2), with $\alpha < 1$ in this example. x_I and I_{gt} are shown sequentially after the target mask m .

3.2.1. Removal Task

For the removal task, i.e., $\epsilon_\theta(\cdot, c_r)$, we set $x_I = I_o$ and $I_{gt} = I_b$ in (1) where $(I_b, I_o, m) \in \mathcal{D}$.

3.2.2. Insertion Task

To train the model for the insertion task, i.e., $\epsilon_\theta(\cdot, c_i)$, we provide x_I in which the object is copy-pasted into the background image with degraded harmonization. Formally, we set the conditional image as:

$$x_I = m \odot C(I_o) + (1 - m) \odot I_b,$$

where \odot denotes the element-wise multiplication and C denotes a degrading operation, randomly chosen between Correlated Color Transform [5] and intensity scaling. To further reflect local light around the inserted region, we apply shadow augmentation to x_I by adjusting the intensity of a partial region of an image. Specifically, for an image I , we define the following shadowing operation:

$$L(I, m_L, \alpha) = m_L \odot (\alpha I) + (1 - m_L) \odot I, \quad (2)$$

m_L is a randomly shaped mask with Gaussian blur and α is an intensity scale. Using the equation (2) and triplet (I_b, I_o, m) , we construct augmented training data for the insertion task as follows: $x_I = m \odot C(I_o) + (1 - m) \odot L(I_b, m_L, \alpha)$, $I_{gt} = L(I_o, m_L, \alpha)$. Figure 3 illustrates an example of the shadowing operation.

3.3. Inference with Controllability

Building on $\epsilon_\theta(\cdot, c_r)$ and $\epsilon_\theta(\cdot, c_i)$, we propose **Cross-Task Guidance (CTG)** to enhance the performance of both removal and insertion tasks through improved controllability. Furthermore, we introduce a spatially extended variant, referred to as **Spatial CTG (S-CTG)**, which enables removal and insertion to be performed on different regions within a single denoising step.

3.3.1. Cross-task Guidance

Relying solely on the conditional outputs $\epsilon_\theta(\cdot, c_r)$ and $\epsilon_\theta(\cdot, c_i)$ may be insufficient to guarantee optimal performance or provide the controllability often needed to reflect user preferences. Classifier-Free Guidance (CFG)[11]

and its variants, which leverage weaker model outputs[1, 14, 17], have demonstrated notable improvements in conditional generation by steering outputs away from unconditional or negatively conditioned references.

In this context, we observe an inherent duality between removal and insertion prompts: the former removes object presence and its visual effects, while the latter synthesizes them. Building on this insight, we introduce **Cross-Task Guidance (CTG)** as follows:

$$\text{(Object removal)} \quad (1 + w)\epsilon_r - w\epsilon_i, \quad (3)$$

$$\text{(Object insertion)} \quad (1 + w)\epsilon_i - w\epsilon_r, \quad (4)$$

where $w > 0$ is a guidance scale, $\epsilon_r = \epsilon_\theta(\cdot, c_r)$, and $\epsilon_i = \epsilon_\theta(\cdot, c_i)$. Each task-specific output is guided by subtracting the output of the opposite task, effectively using it as negative guidance. As illustrated at the top of Figure 2-(b), varying w enables visual effect control.

3.3.2. Spatial Cross-task Guidance for Movement Task

A straightforward approach is to separate the movement task into two stages: object removal followed by object insertion. Let N_r and N_i denote the number of denoising steps required to ensure visual quality in the removal and insertion phases, respectively. This sequential pipeline incurs a total of $N_r + N_i$ inference steps to maintain fidelity across both stages. In contrast, our goal is to achieve object movement within $\max(N_r, N_i)$ steps by jointly leveraging the removal and insertion embeddings, c_r and c_i , in a single denoising process. To this end, we extend CTG to operate in a region-specific manner. Inspired by S-CFG [28], which spatially adjusts the guidance scale of CFG based on semantic segments, we generalize the scalar guidance weight to a matrix form $W \in \mathbb{R}^{h \times w}$.

Specifically, CTG in Equation (3) is applied to \mathcal{P}_r and CTG in Equation (4) is applied to \mathcal{P}_i . As visualized in Figure 2-(b), S-CTG assigns opposite signs to entries in W to apply complementary CTGs to \mathcal{P}_r and \mathcal{P}_i , thereby enabling efficient object movement within a single denoising step. Considering the matrix-scaled guidance:

$$(1 + W) \odot \epsilon_r - W \odot \epsilon_i, \quad (5)$$

we determine each element W_{ij} of the matrix W based on the pixel's membership in \mathcal{P}_r or \mathcal{P}_i , as well as the current denoising step t :

$$W_{ij} = \begin{cases} w_r & \text{if } (i, j) \in \mathcal{P}_r \\ w_i & \text{if } (i, j) \in \mathcal{P}_i \\ \begin{cases} w_r & \text{if } t > t_s \\ w_i & \text{if } t < t_s \end{cases} & \text{if } (i, j) \in \mathcal{P} \setminus (\mathcal{P}_r \cup \mathcal{P}_i) \end{cases}, \quad (6)$$

where \mathcal{P} denotes the set of all pixels, and $w_r > 0$, $w_i < -1$ are the guidance weights for removal and insertion, respectively. The switching step t_s adjusts the *gray area*—pixels belonging to neither \mathcal{P}_r nor \mathcal{P}_i —to prioritize removal during the early denoising steps and insertion during the later steps.

4. Experiments

4.1. Implementations

4.1.1. Training Details

We fine-tune the model on the RORD dataset with a 2:1 ratio of removal to insertion samples, a learning rate of $1e-5$, and an effective batch size of 512 using gradient accumulation. Training is conducted with the Adam optimizer on 8 NVIDIA H100 GPUs.

4.1.2. Evaluation Details

We conduct experiments using a test set with available ground-truth or reference images, and accordingly employ reference-based evaluation metrics such as LPIPS, PSNR, CLIP [23] image score, DINO [6] image score, and FID. For all evaluations, we report the average scores across 10 different random seeds. For in-mask only editing models, we apply additional mask dilation to ensure fair evaluation. For models trained with counterfactual dataset, we fix the dilation size to 10 pixels. We report all parameter tuning details and additional visual results in the Supplementary sections.

4.2. Object Removal

We conduct benchmark experiments for the removal task to evaluate two key aspects: **R1**) object removal performance of CrimEdit and **R2**) the controllability provided by adjusting the CTG scale. For comparison, we employ five baseline methods, categorized as follows: two in-mask editing methods: PowerPoint and ClipAway [10, 42]; one inversion-based method: AttentiveEraser [30]; and two counterfactual-based methods: ROREM and OmniEraser [16, 33].

We use **RemovalBench** [16] as a benchmark for object removal. To address more challenging real-world scenarios, we introduce **BenchHard**, which consists of 100 images—50 drawn from the RORD validation set and 50 captured by professional photographers. Compared to RemovalBench, BenchHard presents more challenging scenarios characterized by (1) larger masks, (2) object removal within repetitive patterns, and (3) complex shadows and reflections. We attached the 100 images in the Supplementary Materials.

Figure 4 and Table 2 show qualitative and quantitative results, respectively, with the CTG scale w to 1.5. It can be observed that (**R1**) CrimEdit outperforms the baselines

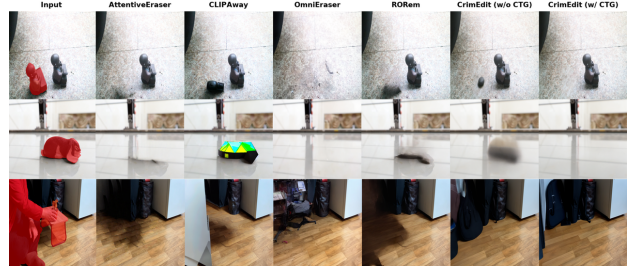


Figure 4. Counterfactual object removal results on BenchHard, which includes challenging scenarios such as repetitive objects (first row), strong reflections (second row), and large mask regions (third row), are shown.

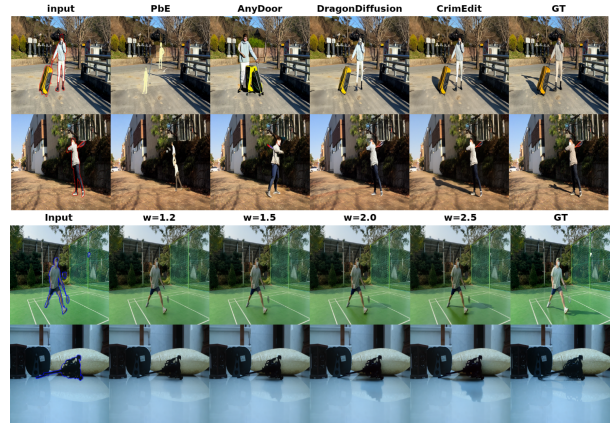


Figure 5. (Top) Object insertion comparison result. (Bottom) Controllability tests on object insertion task.

across most metrics in both benchmarks. As shown in Figure 4, CTG enables the effective removal of both the object and its associated visual effects. To demonstrate **R2**, we plot the results across different CTG scales in Figure 7. We can clearly observe that the results vary with the CTG scale, with a value around 1.5 consistently yielding strong performance across all metrics. These results demonstrate that CTG offers reliable task-specific guidance and enables users to flexibly control the output.

4.3. Object Insertion

To evaluate object insertion performance, we use the RORD validation set, assessing both color harmonization and visual effect generation. To this end, we construct the conditional images (x_I) by copy-pasting target objects from the ground-truth image (I_o) into the background image (I_b) and applying a color transform to the pasted object. We investigate two key aspects: **I1**) whether ϵ_i with CTG achieves performance comparable to existing methods, and **I2**) whether the CTG scale effectively controls the strength of visual effects.

As shown in Table 3 and Figure 5, CrimEdit synthesizes

Table 2. Comparison of object removal performance across two benchmarks.

Algorithm	RemovalBench [16]				BenchHard			
	LPIPS ↓	PSNR ↑	CLIP ↑	DINO ↑	LPIPS ↓	PSNR ↑	CLIP ↑	DINO ↑
PowerPaint	0.346	22.208	96.384	90.791	0.326	19.505	96.369	90.954
CLIPAway	0.396	22.207	96.401	88.934	0.378	19.235	96.124	90.653
OmniEraser	0.377	22.648	97.528	94.156	0.366	21.146	97.255	93.906
Attentive Eraser	0.256	24.515	98.072	94.391	<u>0.235</u>	22.446	97.937	94.416
RORem	<u>0.258</u>	24.262	98.130	94.223	0.243	22.417	98.010	94.613
CrimEdit (w/o CTG)	0.272	24.638	<u>98.787</u>	<u>96.674</u>	0.236	<u>23.194</u>	<u>98.403</u>	<u>96.744</u>
CrimEdit (w/ CTG)	0.271	<u>24.630</u>	98.794	96.717	0.234	23.249	98.523	97.176

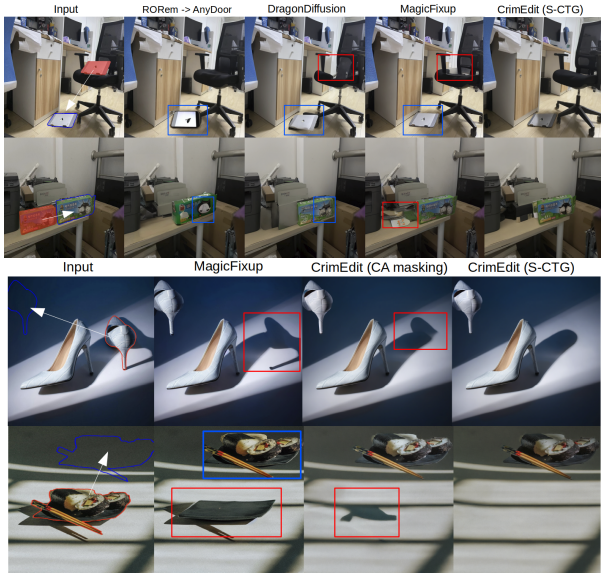


Figure 6. Red boxes indicate unrealistic removal artifacts, while blue boxes denote unrealistic harmonization or effects generation. (Top) Comparison of object movement results on the ReS dataset. (Bottom) Qualitative comparison between CA masking and S-CTG.

more realistic visual effects while better preserving object identity compared to existing methods, thereby validating **I1**. Figure 5 also demonstrates **I2**, where larger guidance scales produce correspondingly larger shadows and reflections. In addition, we measure how the shadow area changes with different CTG scale values, using LISA for shadow detection. In Table 4, PSNR and LPIPS are computed between the output and the original input x_I , restricted to the unmasked region. A larger difference indicates a greater degree of change due to visual effect synthesis. We can observe that larger shadow regions are generated under increased CTG scaling.

Table 3. Object insertion comparative result

	LPIPS ↓	PSNR ↑	CLIP ↑	DINO ↑
PbE	0.418	17.401	93.238	85.602
AnyDoor	0.406	17.252	94.536	89.556
FreeComp.	0.390	19.486	93.300	89.761
Drag.Diff.	0.258	<u>21.039</u>	<u>96.984</u>	<u>94.012</u>
CrimEdit	0.228	22.174	98.055	97.452

Table 4. Shadow Generation Results

CTG scale	Avg. Shad. Pixel Ratio (%)	Ratio of Shad. Det.	PSNR	LPIPS
1.2	0.336	0.27	31.57	0.1741
1.7	0.532	0.33	31.00	0.1848
2.0	0.625	0.41	30.61	0.1941
2.5	0.776	0.42	30.09	0.2163

4.4. Object Movement

We evaluate object movement performance using the ReS dataset [32]. This evaluation focuses on three aspects: **M1**) whether CrimEdit with S-CTG achieves comparable performance to prior methods in counterfactual object repositioning, **M2**) whether it outperforms the cross-attention (CA) masking strategy from FunEditor [26], and **M3**) whether the light adjustment technique in Eq. (2) improves local harmonization. Regarding **M1**, we compare CrimEdit with two open-sourced methods [2, 19]. Additionally, CrimEdit is compared with the result obtained by using separate models for object removal [16] and insertion [7]. The result is shown Table 5 and Figure 6. As shown in Table 5, CrimEdit with S-CTG outperforms other methods with efficient computation times (**M1**). In terms of **M2**, Table 5 and Figure 6 also show the performance gain when using S-CTG rather than CA masking when the same model is used. **M3** is also confirmed by Table 5 where S-CTG shows better performance than the model trained for the same step without light

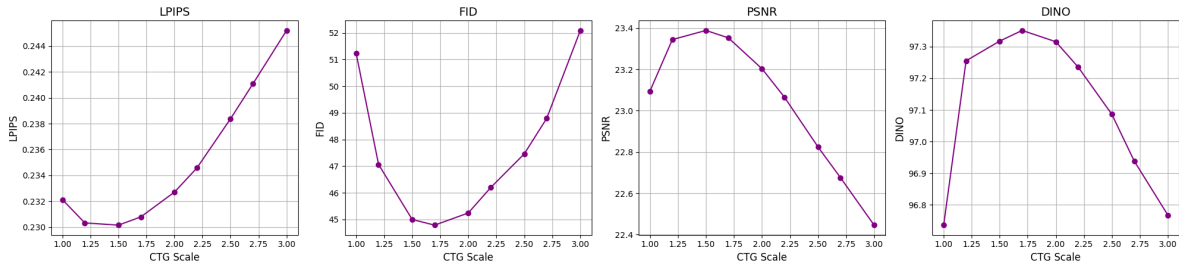


Figure 7. Object removal performance on BenchHard along with CTG scales.

augmentation. More visual results can be found in supplementary material.

Table 5. Object Movement

	LPIPS ↓	PSNR ↑	DINO ↑	T[s] ↓
Anydoor	0.374	18.402	92.501	13.55
Drag.Diff.	0.304	18.294	93.404	16.20
MagicFixup	0.374	19.078	94.384	4.25
Ours (w/o Aug.)	0.289	18.954	94.942	6.74
Ours (CA)	<u>0.291</u>	<u>19.057</u>	<u>95.026</u>	<u>6.65</u>
Ours (S-CTG)	0.286	19.031	95.092	6.74

5. Conclusion

This paper presented a unified diffusion model, CrimEdit, that addresses three image editing tasks—counterfactual object removal, insertion, and movement—by training on two task-specific embeddings, c_r and c_i , derived from a counterfactual dataset. Through the use of Cross-Task Guidance (CTG), CrimEdit demonstrates robust object removal and controllable insertion, particularly in handling visual effects such as shadows. Furthermore, the extension of CTG into its spatial variant, S-CTG, achieves superior performance in object repositioning compared to alternative approaches, including cross-attention masking and separate-stage pipelines

References

- [1] Donghoon Ahn, Hyoungwon Cho, Jaewon Min, Wooseok Jang, Jungwoo Kim, SeonHwa Kim, Hyun Hee Park, Kyong Hwan Jin, and Seungryong Kim. Self-rectifying diffusion sampling with perturbed-attention guidance. In *European Conference on Computer Vision*, pages 1–17. Springer, 2025. 5
- [2] Hadi Alzayer, Zhihao Xia, Xuaner Zhang, Eli Shechtman, Jia-Bin Huang, and Michael Gharbi. Magic fixup: Streamlining photo editing by watching dynamic videos, 2024. 3, 7
- [3] Apple Inc. iphone user guide — edit photos and videos, 2024. Accessed: 2025-04-18. 1
- [4] Omri Avrahami, Dani Lischinski, and Ohad Fried. Blended diffusion for text-driven editing of natural images. In *2022 IEEE/CVF Conference on Computer Vision and Pattern Recognition (CVPR)*, page 18187–18197. IEEE, 2022. 1, 3
- [5] Ákos Borbély, Árpád Sámson, and János Schanda. The concept of correlated colour temperature revisited. *Color Research & Application: Endorsed by Inter-Society Color Council, The Colour Group (Great Britain), Canadian Society for Color, Color Science Association of Japan, Dutch Society for the Study of Color, The Swedish Colour Centre Foundation, Colour Society of Australia, Centre Français de la Couleur*, 26(6):450–457, 2001. 5
- [6] Mathilde Caron, Hugo Touvron, Ishan Misra, Hervé Jégou, Julien Mairal, Piotr Bojanowski, and Armand Joulin. Emerging properties in self-supervised vision transformers. In *Proceedings of the IEEE/CVF international conference on computer vision*, pages 9650–9660, 2021. 6
- [7] Xi Chen, Lianghua Huang, Yu Liu, Yujun Shen, Deli Zhao, and Hengshuang Zhao. Anydoor: Zero-shot object-level image customization, 2024. 3, 7
- [8] Zhekai Chen, Wen Wang, Zhen Yang, Zeqing Yuan, Hao Chen, and Chunhua Shen. Freecompose: Generic zero-shot image composition with diffusion prior, 2024. 3
- [9] Prafulla Dhariwal and Alexander Nichol. Diffusion models beat gans on image synthesis. *Advances in neural information processing systems*, 34:8780–8794, 2021. 1
- [10] Yigit Ekin, Ahmet Burak Yildirim, Erdem Eren Caglar, Aykut Erdem, Erkut Erdem, and Aysegül Dunder. Clipaway: Harmonizing focused embeddings for removing objects via diffusion models, 2024. 3, 6
- [11] Jonathan Ho and Tim Salimans. Classifier-free diffusion guidance. *arXiv preprint arXiv:2207.12598*, 2022. 5
- [12] Haian Jin, Yuan Li, Fujun Luan, Yuanbo Xiangli, Sai Bi, Kai Zhang, Zexiang Xu, Jin Sun, and Noah Snavely. Neural gaffer: Relighting any object via diffusion, 2024. 1
- [13] Xuan Ju, Xian Liu, Xintao Wang, Yuxuan Bian, Ying Shan, and Qiang Xu. Brushnet: A plug-and-play image inpainting model with decomposed dual-branch diffusion, 2024. 1, 3
- [14] Tero Karras, Miika Aittala, Tuomas Kynkäänniemi, Jaakko Lehtinen, Timo Aila, and Samuli Laine. Guiding a diffusion model with a bad version of itself. *arXiv preprint arXiv:2406.02507*, 2024. 5

- [15] Daiqing Li, Aleks Kamko, Ehsan Akhgari, Ali Sabet, Linmiao Xu, and Suhail Doshi. Playground v2.5: Three insights towards enhancing aesthetic quality in text-to-image generation, 2024. 1
- [16] Ruibin Li, Tao Yang, Song Guo, and Lei Zhang. Rorem: Training a robust object remover with human-in-the-loop, 2025. 1, 3, 4, 6, 7
- [17] Tiancheng Li, Weijian Luo, Zhiyang Chen, Liyuan Ma, and Guo-Jun Qi. Self-guidance: Boosting flow and diffusion generation on their own. *arXiv preprint arXiv:2412.05827*, 2024. 5
- [18] Andreas Lugmayr, Martin Danelljan, Andres Romero, Fisher Yu, Radu Timofte, and Luc Van Gool. Repaint: Inpainting using denoising diffusion probabilistic models, 2022. 1, 3
- [19] Chong Mou, Xintao Wang, Jiechong Song, Ying Shan, and Jian Zhang. Dragondiffusion: Enabling drag-style manipulation on diffusion models, 2023. 1, 3, 7
- [20] Chong Mou, Xintao Wang, Jiechong Song, Ying Shan, and Jian Zhang. Diffeditor: Boosting accuracy and flexibility on diffusion-based image editing, 2024. 3
- [21] William Peebles and Saining Xie. Scalable diffusion models with transformers. In *Proceedings of the IEEE/CVF International Conference on Computer Vision*, pages 4195–4205, 2023. 1
- [22] Dustin Podell, Zion English, Kyle Lacey, Andreas Blattmann, Tim Dockhorn, Jonas Müller, Joe Penna, and Robin Rombach. Sdxl: Improving latent diffusion models for high-resolution image synthesis. *arXiv preprint arXiv:2307.01952*, 2023. 1, 4
- [23] Alec Radford, Jong Wook Kim, Chris Hallacy, Aditya Ramesh, Gabriel Goh, Sandhini Agarwal, Girish Sastry, Amanda Askell, Pamela Mishkin, Jack Clark, et al. Learning transferable visual models from natural language supervision. In *International conference on machine learning*, pages 8748–8763. PmLR, 2021. 6
- [24] Robin Rombach, Andreas Blattmann, Dominik Lorenz, Patrick Esser, and Björn Ommer. High-resolution image synthesis with latent diffusion models. In *Proceedings of the IEEE/CVF conference on computer vision and pattern recognition*, pages 10684–10695, 2022. 1
- [25] Min-Cheol Sagong, Yoon-Jae Yeo, Seung-Won Jung, and Sung-Jea Ko. Rord: A real-world object removal dataset. In *BMVC*, page 542, 2022. 1, 2, 3, 4
- [26] Mohammadreza Samadi, Fred X. Han, Mohammad Salameh, Hao Wu, Fengyu Sun, Chunhua Zhou, and Di Niu. Funeditor: Achieving complex image edits via function aggregation with diffusion models, 2024. 3, 7
- [27] Samsung. How to use generative photo editing on the galaxy s24, 2024. Accessed: 2025-04-18. 1
- [28] Dazhong Shen, Guanglu Song, Zeyue Xue, Fu-Yun Wang, and Yu Liu. Rethinking the spatial inconsistency in classifier-free diffusion guidance. In *Proceedings of The IEEE/CVF Computer Vision and Pattern Recognition Conference (CVPR)*, 2024. 5
- [29] Yizhi Song, Zhifei Zhang, Zhe Lin, Scott Cohen, Brian Price, Jianming Zhang, Soo Ye Kim, and Daniel Aliaga. Object-stitch: Generative object compositing, 2022. 1, 3
- [30] Wenhao Sun, Benlei Cui, Xue-Mei Dong, Jingqun Tang, and Yi Liu. Attentive eraser: Unleashing diffusion model’s object removal potential via self-attention redirection guidance, 2025. 3, 6
- [31] Tianyu Wang, Jianming Zhang, Haitian Zheng, Zhihong Ding, Scott Cohen, Zhe Lin, Wei Xiong, Chi-Wing Fu, Luis Figueroa, and Soo Ye Kim. Metashadow: Object-centered shadow detection, removal, and synthesis, 2024. 3
- [32] Yikai Wang, Chenjie Cao, Ke Fan, Qiaole Dong, Yifan Li, Xiangyang Xue, and Yanwei Fu. Repositioning the subject within image, 2024. 1, 3, 7
- [33] Runpu Wei, Zijin Yin, Shuo Zhang, Lanxiang Zhou, Xueyi Wang, Chao Ban, Tianwei Cao, Hao Sun, Zhongjiang He, Kongming Liang, and Zhanyu Ma. Omnieraser: Remove objects and their effects in images with paired video-frame data, 2025. 1, 3, 6
- [34] Daniel Winter, Matan Cohen, Shlomi Fruchter, Yael Pritch, Alex Rav-Acha, and Yedid Hoshen. Objectdrop: Bootstrapping counterfactuals for photorealistic object removal and insertion, 2024. 1, 3, 4
- [35] Shaoan Xie, Zhifei Zhang, Zhe Lin, Tobias Hinz, and Kun Zhang. Smartbrush: Text and shape guided object inpainting with diffusion model, 2022. 1, 3
- [36] Binxin Yang, Shuyang Gu, Bo Zhang, Ting Zhang, Xuejin Chen, Xiaoyan Sun, Dong Chen, and Fang Wen. Paint by example: Exemplar-based image editing with diffusion models, 2022. 1, 3
- [37] Siyuan Yang, Lu Zhang, Liqian Ma, Yu Liu, JingJing Fu, and You He. Magicremover: Tuning-free text-guided image inpainting with diffusion models, 2023. 1, 3
- [38] Xin Yu, Tianyu Wang, Soo Ye Kim, Paul Guerrero, Xi Chen, Qing Liu, Zhe Lin, and Xiaojuan Qi. Objectmover: Generative object movement with video prior, 2025. 1, 3
- [39] Yongsheng Yu, Ziyun Zeng, Haitian Zheng, and Jiebo Luo. Omnipaint: Mastering object-oriented editing via disentangled insertion-removal inpainting, 2025. 1, 3
- [40] Lvmin Zhang, Anyi Rao, and Maneesh Agrawala. Scaling in-the-wild training for diffusion-based illumination harmonization and editing by imposing consistent light transport. In *The Thirteenth International Conference on Learning Representations*, 2025. 1
- [41] Jixin Zhao, Shangchen Zhou, Zhouxia Wang, Peiqing Yang, and Chen Change Loy. Objectclear: Complete object removal via object-effect attention, 2025. 4
- [42] Junhao Zhuang, Yanhong Zeng, Wenran Liu, Chun Yuan, and Kai Chen. A task is worth one word: Learning with task prompts for high-quality versatile image inpainting, 2024. 1, 3, 6

Supplementary Material

6. Additional Ablations

6.1. Light augmentation in Movement

As stated in equation (2), CrimEdit adopted optional lighting augmentation. Qualitative comparison is shown in Figure 8.



Figure 8. Comparison result for the light augmentation.

6.2. Separate-phased Approach in Movement

Using ReS dataset, we compare S-CTG with the separate-phased approach consisting of object removal and insertion. The latter approach is given the total $N_r + N_i = 50$ denoising step where N_r is the steps used for removal and N_i for insertion. We used the same model and CTG scale 1.5 was applied for each phase. Figure 9 and 10 shows that S-CTG yielded better results for the visual quality and perceptual metrics.

7. Additional Qualitative Results

In this section, we include more visual results to access the proposed methods. Figure 11 shows the comparative results showing the superior performance of the proposed CTG method. Figure 12 and Figure 13 depict the comparative result and the effect of the CTG scale in the insertion task. As Figure 13 shows, a higher CTG scale produces larger shadow mask.

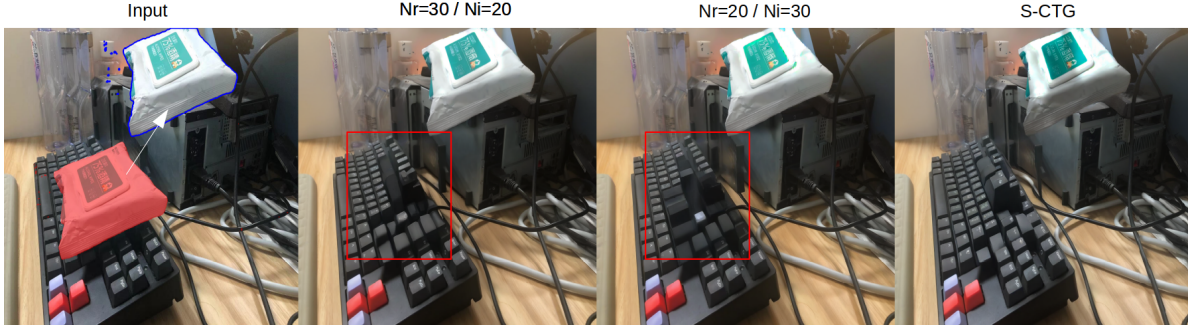


Figure 9. Visual comparison with separate-phased approach. The box regions show that small amount of denoising steps for removal can lead to blurry result.

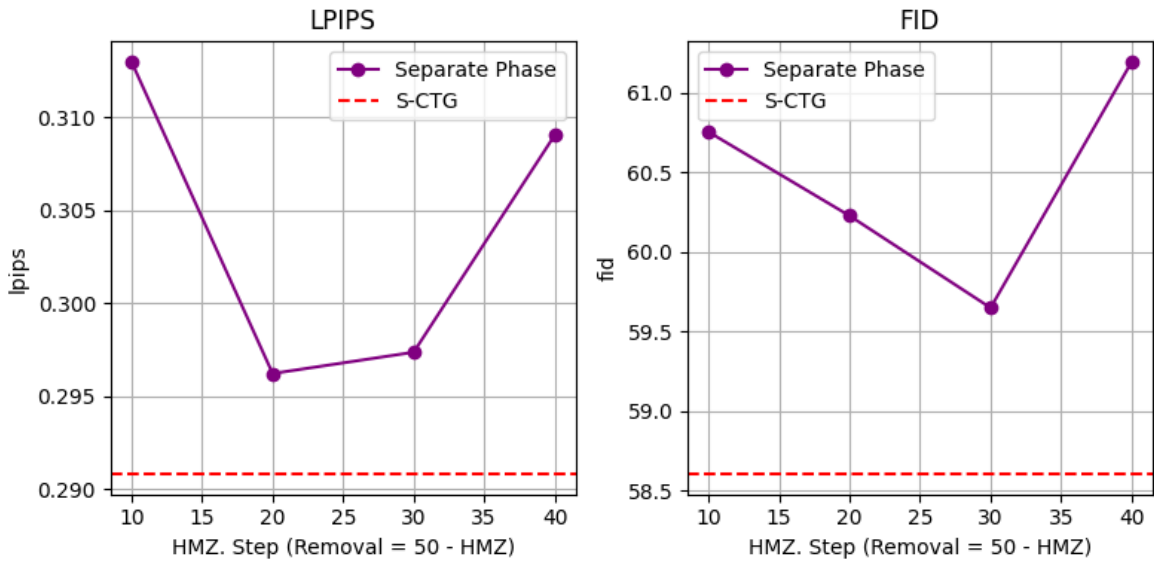


Figure 10. Comparison with separate-phased approach.

8. Evaluation Details

8.1. BenchHard Dataset

8.2. Parameter Tuning of Baselines

We tuned the other arts by finding the parameter set that best rewards the sum of the metric set in a normalized scale. This section shows the turning history and their selected parameters, shown in a boldface.

Table 6. PowerPoint (Left: BenchHard / Right: RemovalBench)

Dilation	Scale	LPIPS	FID	PSNR	CLIP	DINO	Dilation	Scale	LPIPS	FID	PSNR	CLIP	DINO
10	10.5	0.3255	108.09	19.40	96.24	90.81	10	10.5	0.3470	135.22	21.95	96.27	90.18
10	13.5	0.3291	108.89	19.28	96.10	90.65	10	13.5	0.3515	142.27	21.71	96.11	89.94
15	10.5	0.3264	105.52	19.50	96.37	90.95	15	10.5	0.3462	123.78	22.21	96.38	90.79
15	13.5	0.3300	107.75	19.35	96.21	90.76	15	13.5	0.3511	135.00	21.92	96.14	90.53

Table 7. CLIPAway Results: (Left: BenchHard / Right: RemovalBench)

Dilation	Scale	LPIPS	FID	PSNR	CLIP	DINO	Dilation	Scale	LPIPS	FID	PSNR	CLIP	DINO
10	0.5	0.3751	112.34	19.30	96.11	89.84	10	0.5	0.3957	132.51	22.12	96.29	88.40
10	1.0	0.3783	110.66	19.23	96.12	90.65	10	1.0	0.3980	130.70	22.05	96.32	89.12
10	1.5	0.3822	109.55	19.07	96.06	90.51	10	1.5	0.4012	133.89	21.76	96.09	89.13
15	0.5	0.3778	113.04	19.24	96.07	89.64	15	0.5	0.3957	121.60	22.21	96.40	88.93
15	1.0	0.3810	112.24	19.21	96.11	90.44	15	1.0	0.3981	122.68	22.13	96.32	89.79
15	1.5	0.3864	114.86	18.98	95.92	90.13	15	1.5	0.4015	124.65	21.85	96.22	89.78

Table 8. OmniEraser Results: (Left: BenchHard / Right: RemovalBench)

CFG scale	LPIPS	FID	PSNR	CLIP	DINO	Scale	LPIPS	FID	PSNR	CLIP	DINO
1.0	0.6173	265.49	14.19	86.75	69.99	1.0	0.6567	336.11	14.74	87.84	67.66
2.0	0.6261	246.16	13.32	86.93	73.16	2.0	0.6816	325.31	13.55	86.68	70.92
3.5	0.3663	77.76	21.15	97.25	93.91	3.5	0.3774	70.88	22.65	97.53	94.16
7.0	0.6390	230.97	13.83	88.36	74.87	7.0	0.6940	309.08	13.88	88.14	72.85

Table 9. RORem Results: (Left: BenchHard / Right: RemovalBench)

CFG	LPIPS	FID	PSNR	CLIP	DINO	CFG	LPIPS	FID	PSNR	CLIP	DINO
1	0.2429	64.15	22.42	98.01	94.61	1	0.2577	83.02	24.24	98.12	94.14
3	0.2436	64.10	22.40	98.01	94.58	3	0.2576	82.79	24.25	98.12	94.21
5	0.2438	64.12	22.38	98.00	94.55	5	0.2577	82.66	24.26	98.13	94.22
7	0.2449	64.81	22.34	97.99	94.47	7	0.2578	82.90	24.27	98.13	94.22
9	0.2464	65.58	22.30	97.98	94.38	9	0.2587	83.12	24.26	98.12	94.19

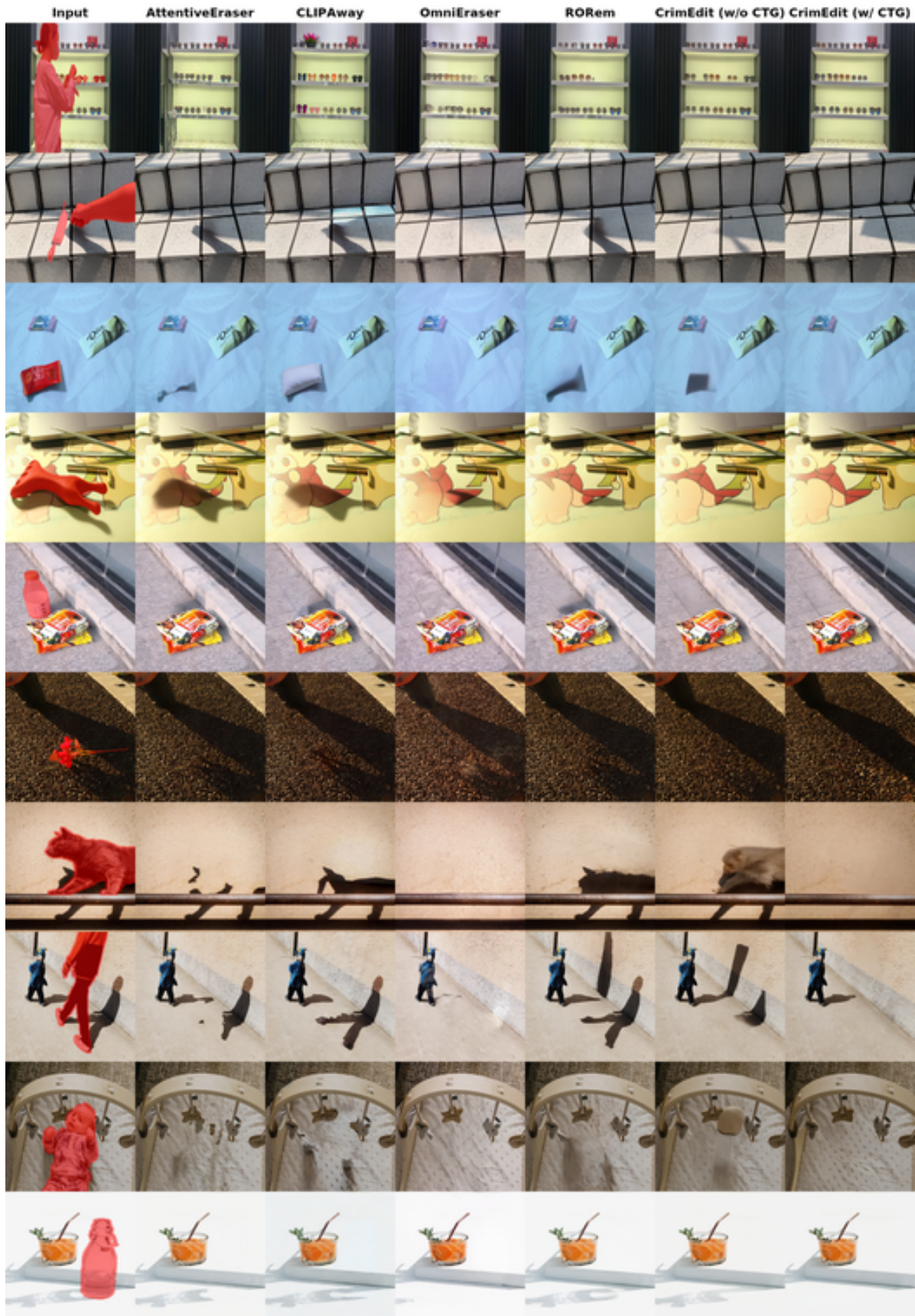


Figure 11. Qualitative comparison for the counterfactual removal for BenchHard dataset. The models are given the red-shaded mask only, without including the visual effects.



Figure 12. Qualitative comparison for the counterfactual insertion for RORD validation set.

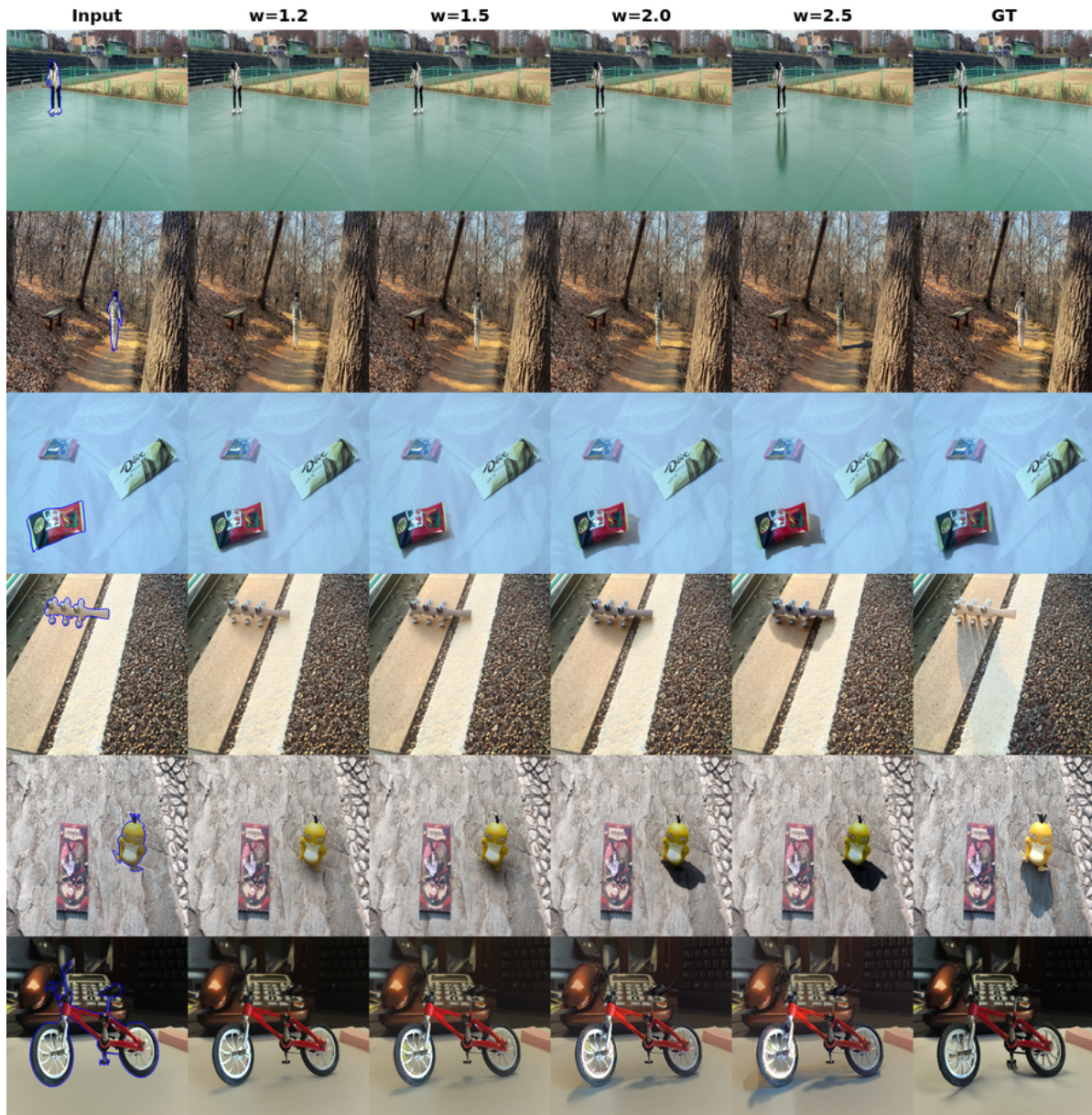


Figure 13. Controllability test for insertion task by changing the CTG weight.

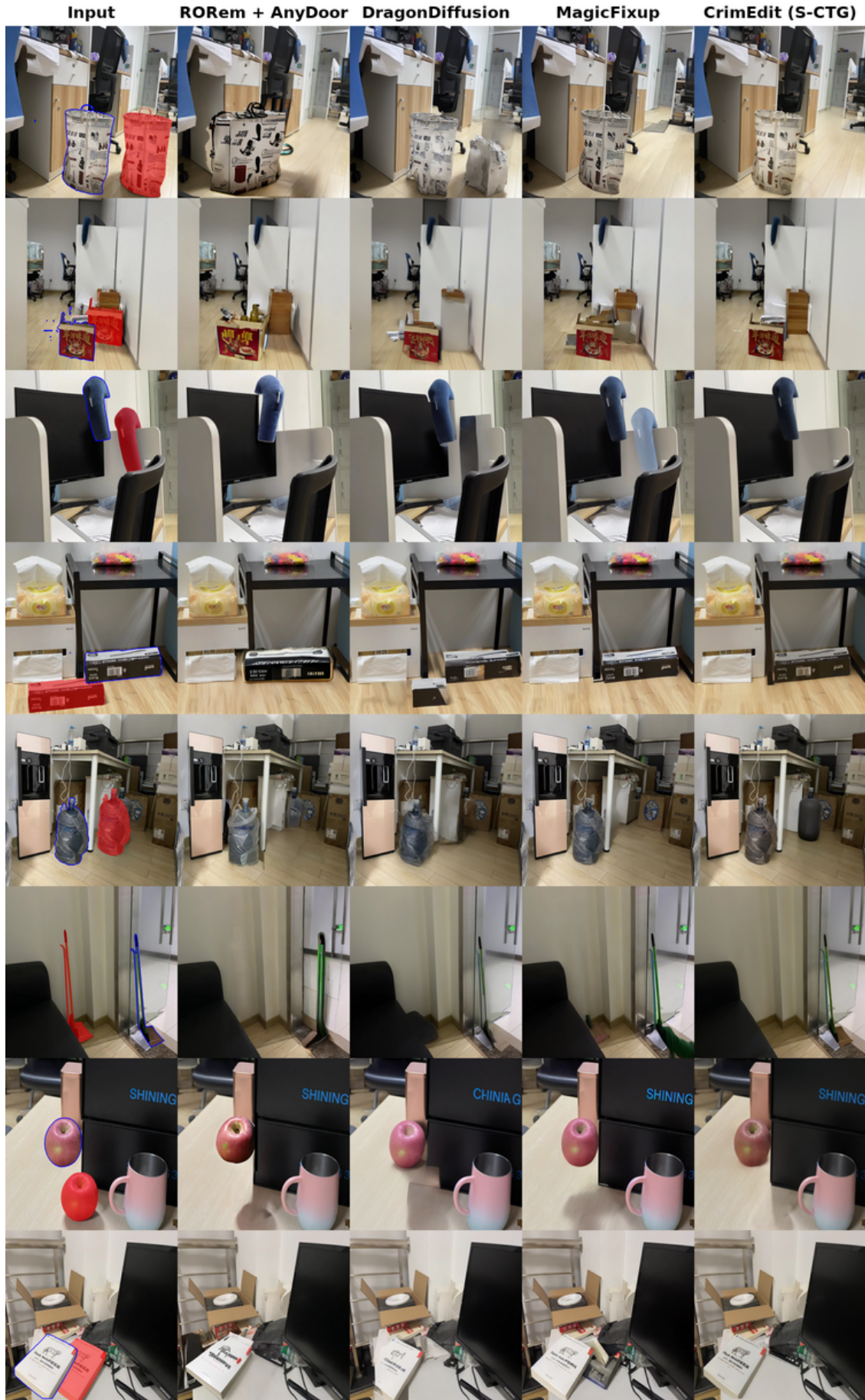


Figure 14. Object movement comparative results.



Figure 15. 100 images of BenchHard. Red shade visualizes the given masks.

cfg	Rem. guidance	Similarity supp. steps	Similarity supp. scale	strength	LPIPS	FID	PSNR	CLIP	DINO
1.0	7	5	0.3	0.8	0.2353	64.5465	22.4108	97.9236	94.2675
1.0	7	5	0.3	0.9	0.2354	64.5416	22.4144	97.9399	94.3148
1.0	7	5	0.3	1.0	0.2360	64.7933	22.3893	97.9089	94.2402
1.0	7	5	0.5	0.8	0.2359	66.5109	22.2117	97.8727	94.2292
1.0	7	5	0.5	0.9	0.2358	62.9151	22.3571	97.9553	94.2937
1.0	7	5	0.5	1.0	0.2360	64.5297	22.3854	97.9248	94.3316
1.0	7	9	0.3	0.8	0.2352	65.7186	22.4169	97.8995	94.1419
1.0	7	9	0.3	0.9	0.2353	66.3822	22.4285	97.8630	94.2854
1.0	7	9	0.3	1.0	0.2358	63.4083	22.4153	97.9072	94.1839
1.0	7	9	0.5	0.8	0.2354	65.6787	22.4187	97.9326	94.3263
1.0	7	9	0.5	0.9	0.2353	65.1219	22.4715	97.9290	94.2453
1.0	7	9	0.5	1.0	0.2357	65.8562	22.4509	97.8830	94.2129
1.0	9	5	0.3	0.8	0.2354	65.8350	22.4294	97.8846	94.3280
1.0	9	5	0.3	0.9	0.2354	64.9290	22.4649	97.9011	94.1800
1.0	9	5	0.3	1.0	0.2358	64.5543	22.3940	97.9390	94.4061
1.0	9	5	0.5	0.8	0.2355	66.9499	22.3768	97.9633	94.2039
1.0	9	5	0.5	0.9	0.2357	64.9623	22.4054	97.9788	94.2309
1.0	9	5	0.5	1.0	0.2358	64.7565	22.3793	97.9191	94.3760
1.0	9	9	0.3	0.8	0.2354	65.6625	22.4099	97.8594	94.1816
1.0	9	9	0.3	0.9	0.2356	64.9122	22.4341	97.8966	94.1760
1.0	9	9	0.3	1.0	0.2358	64.5817	22.4314	97.8888	94.2095
1.0	9	9	0.5	0.8	0.2890	68.0023	21.0889	96.4145	90.3991
1.0	9	9	0.5	0.9	0.2356	64.7674	22.4499	97.9156	94.2936
1.0	9	9	0.5	1.0	0.2358	64.9755	22.4365	97.8997	94.2588
2.0	7	5	0.3	0.8	0.2353	64.5465	22.4108	97.9236	94.2675
2.0	7	5	0.3	0.9	0.2354	64.5416	22.4144	97.9399	94.3148
2.0	7	5	0.3	1.0	0.2360	64.7933	22.3893	97.9089	94.2402
2.0	7	5	0.5	0.8	0.2359	66.5109	22.2117	97.8727	94.2292
2.0	7	5	0.5	0.9	0.2358	62.9151	22.3571	97.9553	94.2937
2.0	7	5	0.5	1.0	0.2360	64.5297	22.3854	97.9248	94.3316
2.0	7	9	0.3	0.8	0.2352	65.7186	22.4169	97.8995	94.1419
2.0	7	9	0.3	0.9	0.2353	66.3822	22.4285	97.8630	94.2854
2.0	7	9	0.3	1.0	0.2358	63.4083	22.4153	97.9072	94.1839
2.0	7	9	0.5	0.8	0.2354	65.6787	22.4187	97.9326	94.3263
2.0	7	9	0.5	0.9	0.2353	65.1219	22.4715	97.9290	94.2453
2.0	7	9	0.5	1.0	0.2357	65.8562	22.4509	97.8830	94.2129
2.0	9	5	0.3	0.8	0.2354	65.8350	22.4294	97.8846	94.3280
2.0	9	5	0.3	0.9	0.2354	64.9290	22.4649	97.9011	94.1800
2.0	9	5	0.3	1.0	0.2358	64.5543	22.3940	97.9390	94.4061
2.0	9	5	0.5	0.8	0.2355	66.9499	22.3768	97.9633	94.2039
2.0	9	5	0.5	0.9	0.2357	64.9623	22.4054	97.9788	94.2309
2.0	9	5	0.5	1.0	0.2358	64.7565	22.3793	97.9191	94.3760
2.0	9	9	0.3	0.8	0.2354	65.6625	22.4099	97.8594	94.1816
2.0	9	9	0.3	0.9	0.2356	64.9122	22.4341	97.8966	94.1760
2.0	9	9	0.3	1.0	0.2358	64.5817	22.4314	97.8888	94.2095
2.0	9	9	0.5	0.8	0.2354	65.4113	22.4455	97.9366	94.4160
2.0	9	9	0.5	0.9	0.2356	64.7674	22.4499	97.9156	94.2936
2.0	9	9	0.5	1.0	0.2358	64.9755	22.4365	97.8997	94.2588

Table 10. Attentive Eraser (BenchHard)

cfg	Rem. guidance	Similarity supp. steps	Similarity supp. scale	strength	LPIPS	FID	PSNR	CLIP	DINO
1.0	7	5	0.3	0.8	0.2559	79.5612	24.4449	98.0463	94.2709
1.0	7	5	0.3	0.9	0.2557	77.4792	24.4695	98.0507	94.1880
1.0	7	5	0.3	1.0	0.2557	78.5954	24.5227	98.0533	94.0470
1.0	7	5	0.5	0.8	0.2561	78.7337	24.4234	98.0707	94.1455
1.0	7	5	0.5	0.9	0.2556	78.2796	24.4913	98.0245	94.2425
1.0	7	5	0.5	1.0	0.2557	77.6969	24.5258	98.0491	94.0396
1.0	7	9	0.3	0.8	0.2560	79.4169	24.5148	98.0897	94.1993
1.0	7	9	0.3	0.9	0.2559	77.9213	24.5126	98.0758	94.2251
1.0	7	9	0.3	1.0	0.2558	78.3305	24.4982	98.0413	94.1997
1.0	7	9	0.5	0.8	0.2558	80.0599	24.4904	98.0713	94.2864
1.0	7	9	0.5	0.9	0.2557	78.0075	24.5081	98.0631	94.2688
1.0	7	9	0.5	1.0	0.2557	76.3665	24.5213	98.0488	94.1518
1.0	9	5	0.3	0.8	0.2558	79.8573	24.5034	98.0514	94.3472
1.0	9	5	0.3	0.9	0.2558	78.5669	24.4793	98.0416	94.2727
1.0	9	5	0.3	1.0	0.2557	77.1161	24.5108	98.0483	93.9702
1.0	9	5	0.5	0.8	0.2558	79.4824	24.4835	98.0598	94.3191
1.0	9	5	0.5	0.9	0.2557	77.6902	24.5004	98.0346	94.2263
1.0	9	5	0.5	1.0	0.2557	77.3909	24.5164	98.0558	94.0791
1.0	9	9	0.3	0.8	0.2562	78.8775	24.5164	98.0217	94.2556
1.0	9	9	0.3	0.9	0.2560	78.7569	24.5121	98.0703	94.3393
1.0	9	9	0.3	1.0	0.2558	77.8419	24.5052	98.0490	94.1366
1.0	9	9	0.5	0.8	0.2562	79.0362	24.4625	98.0156	94.0172
1.0	9	9	0.5	0.9	0.2558	77.7559	24.5118	98.0638	94.3270
1.0	9	9	0.5	1.0	0.2557	77.1574	24.5194	98.0535	94.1307
2.0	7	5	0.3	0.8	0.2559	79.5612	24.4449	98.0463	94.2709
2.0	7	5	0.3	0.9	0.2557	77.4792	24.4695	98.0507	94.1880
2.0	7	5	0.3	1.0	0.2557	78.5954	24.5227	98.0533	94.0470
2.0	7	5	0.5	0.8	0.2561	78.7337	24.4234	98.0707	94.1455
2.0	7	5	0.5	0.9	0.2556	78.2796	24.4913	98.0245	94.2425
2.0	7	5	0.5	1.0	0.2557	77.6969	24.5258	98.0491	94.0396
2.0	7	9	0.3	0.8	0.2560	79.4169	24.5148	98.0897	94.1993
2.0	7	9	0.3	0.9	0.2559	77.9213	24.5126	98.0758	94.2251
2.0	7	9	0.3	1.0	0.2558	78.3305	24.4982	98.0413	94.1997
2.0	7	9	0.5	0.8	0.2558	80.0599	24.4904	98.0713	94.2864
2.0	7	9	0.5	0.9	0.2557	78.0075	24.5081	98.0631	94.2688
2.0	7	9	0.5	1.0	0.2557	76.3665	24.5213	98.0488	94.1518
2.0	9	5	0.3	0.8	0.2558	79.8573	24.5034	98.0514	94.3472
2.0	9	5	0.3	0.9	0.2558	78.5669	24.4793	98.0416	94.2727
2.0	9	5	0.3	1.0	0.2557	77.1161	24.5108	98.0483	93.9702
2.0	9	5	0.5	0.8	0.2558	79.4824	24.4835	98.0598	94.3191
2.0	9	5	0.5	0.9	0.2557	77.6902	24.5004	98.0346	94.2263
2.0	9	5	0.5	1.0	0.2557	77.3909	24.5164	98.0558	94.0791
2.0	9	9	0.3	0.8	0.2562	78.8775	24.5164	98.0217	94.2556
2.0	9	9	0.3	0.9	0.2560	78.7569	24.5121	98.0703	94.3393
2.0	9	9	0.3	1.0	0.2558	77.8419	24.5052	98.0490	94.1366
2.0	9	9	0.5	0.8	0.2557	78.5961	24.5152	98.0720	94.3913
2.0	9	9	0.5	0.9	0.2558	77.7559	24.5118	98.0638	94.3270
2.0	9	9	0.5	1.0	0.2557	77.1574	24.5194	98.0535	94.1307

Table 11. Attentive Eraser (RemovalBench)

Table 12. Tuning of insertion algorithm on RORD validation set.

FreeCompose						AnyDoor						
DDS weight	LPIPS	FID	PSNR	CLIP	DINO	Guidance scale	Control scale	LPIPS	FID	PSNR	CLIP	DINO
1.0	0.3927	120.2	19.47	93.25	89.71	1.0	0.4	0.4807	193.9	15.63	88.45	75.74
1.5	0.3901	119.9	19.49	93.30	89.76	1.0	0.8	0.4203	136.0	17.16	92.77	83.40
2.0	0.3904	120.0	19.48	93.29	89.70	1.0	1.0	0.4076	130.9	17.36	93.70	84.63
Paint-by-Example						1.0	1.2	0.4093	141.7	17.25	93.76	85.43
CFG scale	LPIPS	FID	PSNR	CLIP	DINO	1.0	1.5	0.4252	157.5	16.63	93.11	84.84
1.0	0.4190	146.0	17.54	91.87	82.59	1.0	2.0	0.4699	177.9	15.50	90.90	80.47
3.0	0.4183	135.1	17.47	92.98	84.99	4.5	0.4	0.4776	150.7	15.36	90.86	82.09
5.0	0.4182	133.0	17.40	93.24	85.60	4.5	0.8	0.4184	123.0	17.10	94.17	88.43
7.0	0.4183	132.6	17.34	93.30	85.91	4.5	1.0	0.4065	130.2	17.25	94.54	89.56
9.0	0.4185	131.7	17.29	93.34	86.06	4.5	1.2	0.4224	122.2	16.67	94.23	89.28
						4.5	1.5	0.4430	125.0	15.88	93.81	89.02
						4.5	2.0	0.4710	138.4	15.12	92.97	87.64
						7.0	0.4	0.4710	164.6	15.46	91.45	83.03
						7.0	0.8	0.4248	125.2	16.90	94.00	88.38
						7.0	1.0	0.4136	132.2	16.99	94.34	89.55
						7.0	1.2	0.4309	126.2	16.42	93.93	89.29
						7.0	1.5	0.4414	145.7	15.88	93.52	89.23
						7.0	2.0	0.4835	133.6	14.78	92.52	87.22

$w_{content}$	$w_{contrast}$	w_{id}	Guidance scale	Energy scale	LPIPS	FID	PSNR	CLIP	DINO
3	0.1	1.8	7	0.9	0.3093	68.2051	18.2531	96.7788	92.8310
3	0.1	1.8	7	1.5	0.3068	66.8024	18.2299	96.8619	93.0648
3	0.1	2.5	7	0.9	0.3092	68.4845	18.2347	96.7950	92.7789
3	0.1	2.5	7	1.5	0.3081	67.3742	18.1283	96.8288	92.9424
3	0.2	1.8	7	0.9	0.3103	68.9174	18.2117	96.7664	92.7191
3	0.2	1.8	7	1.5	0.3079	67.7704	18.1751	96.8291	92.9493
3	0.2	2.5	7	0.9	0.3101	69.0386	18.2018	96.7840	92.6634
3	0.2	2.5	7	1.5	0.3094	68.1056	18.0344	96.8164	92.8475
3	0.3	1.8	7	0.9	0.3113	69.9344	18.1741	96.7384	92.6562
3	0.3	1.8	7	1.5	0.3090	68.1417	18.1031	96.8240	92.8750
3	0.3	2.5	7	0.9	0.3112	69.8445	18.1593	96.7535	92.6027
3	0.3	2.5	7	1.5	0.3103	69.0084	17.9881	96.8104	92.8011
6	0.1	1.8	7	0.9	0.3047	65.8831	18.3690	96.8665	93.2757
6	0.1	1.8	7	1.5	0.3038	64.8498	18.2943	96.9336	93.4044
6	0.1	2.5	7	0.9	0.3047	66.1367	18.3477	96.8574	93.2554
6	0.1	2.5	7	1.5	0.3058	66.0787	18.1736	96.8706	93.1908
6	0.2	1.8	7	0.9	0.3051	66.2827	18.3445	96.8646	93.1979
6	0.2	1.8	7	1.5	0.3047	65.7645	18.2499	96.9187	93.3180
6	0.2	2.5	7	0.9	0.3052	66.4090	18.3242	96.8693	93.0798
6	0.2	2.5	7	1.5	0.3059	66.6991	18.1355	96.8560	93.1302
6	0.3	1.8	7	0.9	0.3065	73.7313	18.3854	96.8271	93.0749

Table 13. DragonDiffusion